Sand deformation around growing maize roots: an investigation with x-ray tomography

Anselmucci Floriana, Andò Edward, Viggiani Gioacchino, Lenoir Nicolas, Peyroux Robert, Arson Chloé, Sibille Luc

Abstract

Effects of root growth on soil has an important role in soil strength as is thus of interest for geotechnical engineering. This paper reveals the importance of initial bulk density on the response of soil to plant root evolution. Root-soil interaction is investigated through the growth of maize roots in sand with two bulk densities. A 3D timeseries of the root-soil interaction is imaged using x-ray computed tomography, to observe micro-scale interaction for 8 days. Using digital image correlation, the total strain fields is obtained. The root system shears the soil and the propagation of the shear effect results to be larger when the bulk density is lower. Volumetric deformation in the sand is investigated. It is concluded that the sheared volume presents different volumetric responses according to the initial density. In the vicinity of the root the soil dilates, but lower is the initial density, more the soil tends to compact with respect to distance from the root surface.

Background

The mechanical interactions of a growing root with the surrounding soil are complex. There are many factors at play: the mechanical properties of the soil and its initial state (density, pore size distribution, water content), the root itself (hairs and exudates of the root (Koebernick et al. 2017, Carminati & Vetterlein 2013), the loss of the pore water due to evapotranspiration, the ratio of root diameter to typical pore size, and the connectivity of the soil macroporosity Lucas et al. 2019. To penetrate a soil, an individual root must either displace soil material by a combination of rigid-body movement, shear, and compression (Bengough et al. 2011) or follow the path of an existing pore network (White & Kirkegaard 2010) (if the root can fit inside the pores), all of these actions modify the microstructure of the surrounding soil, and thus alter its mechanical and physical properties.

Most of the previous studies focused on the effect that roots have on the soil physical properties up to few millimetres from the root (rhizosphere). As roots mature, their growth and their exudates alter the soil water potential (Hinsinger et al. 2009). Rhizosphere properties evolve in time, depending on the root age (Carminati & Vetterlein 2013), without omitting the importance

of root-hairs presence, they improve root-soil contact and increase the soil aggregation (Moreno-Espíndola et al. 2007). The impact of roots on soil porosity in the rhizosphere has been importantly investigated. An increase of the macro-porosity of the soil in direct contact with the root is often observed (Helliwell et al. 2019). (Helliwell et al. 2017) explained such an increase of porosity due to the geometrical constraint brought by the root, grains pack more loosely near a flat object (root) than against other grains. Further in the rhizosphere, the change of porosity may be either positive or negative (Tracy et al. 2012). Nevertheless such modifications of the porosity of the soils, and how it evolves with the distance from the root, depend on the initial soil density, the connectivity of the macropores (Lucas et al. 2019, Helliwell et al. 2019), and the root density (Bodner et al. 2014). Besides, in some cases, investigation tools may affect the results. Mooney et al. (2012) reviewed the application of x-ray Computed Tomography (XRCT) in root visualisation studies in the last 40 years, and concluded that XRCT has a good potential to unravel the complex interaction between roots and soil. Finally, Keyes et al. (2016, 2017) used in-vivo XRCT combined with digital image correlation to map soil deformation around a growing root tip at different time steps, with a particular emphasis on the tip of the root.

In the present study, we study deformation and microstructure changes induced by a maize root growing in sand, not only in the vicinity of the root, but also outside the rhizosphere. Within the first few days of plant growth, we used in-vivo 4D x-ray microtomography and 3D digital image correlation to observe and measure the kinematics of the root-sand system with time.

Granular material preparation

The soil used is Hostun HN31 sand, a fine-grained, angular siliceous sand coming from the Hostun quarry (Drôme, France) which is operated by Sibelco. Table 1 summarises its index properties (Canou 1989, Flavigny et al. 1990).

	D_{50}[mm]	Cu	C_g	e_{min}	e_{max}	G_s
HN31	0.338	1.5	1	0.648	1.041	2.65

Table 1: Hostun sand index properties: mean grain size D_{50}, coefficient of uniformity Cu = D_{60}/D_{10}, Coefficient of gradation $C_g = (D_{30})^2/ (D_{60}D_{10})$, minimum and maximum void ratio, and the specific gravity G_s (Canou 1989, Flavigny et al. 1990)

The sand is dry pluviated into a cylindrical poly-methyl methacrylate (PMMA) tube, the diameter of which is chosen to optimise the trade-off between pixel size and field of view during x-ray imaging (which encourages small diameters for small pixel sizes), as well to avoid strong boundary effects during pluviation and root growth (which encourages larger diameters). After a series of trials, a diameter of 50 mm and a height of 100 mm were selected. Pluviation was performed with drop heights of 2 mm and 100 mm yielded relative densities D_R of 30% and 80%. Table 2 summarises the pluviation parameters used.

Seed preparation

Among crops generating fibrous root system architecture, a wild-type of maize (Zea Mays L.) is used for this study. The root system of Zea Mays L. has a unique architecture which secures the

Pluviation parameters	Looser Dr=30%	Denser Dr=80%
drop height [mm]	2	100
opening width funnel [mm]	7	7
pouring rate [cm^3/s]	1.51-1.64	2.45-2.80

Table 2: Summary of pluviation parameters

efficient uptake of water and nutrients and provides anchorage (Lynch 1995). Seeds are sterilised in a solution of 15% bleach in distilled water for 15 minutes then rinsed in distilled water. Thereafter, seeds are transferred in culture dishes between wet filter papers, foil-wrapped and germinated for 48-60 hours at a fixed temperature of $19\,°C\pm2\,°C$. Seeds with a germinated root, called radicle, of about 10-15 mm in length are selected to be studied.

Granular sample preparation with seed

The germinated seed is radially centred in the cylindrical tube during sand pluviation at a depth of 1.5 to 2 times the seed diameter. The radicle is always pointing downward. A base was specifically designed with a pattern of holes which enables sample watering from the bottom, by capillarity. Watering is done on a 7-days basis. Unlike field soil, sand cannot provide any nutrients for the root system. The water provided to the seed is consequently enriched with soluble plant feed (detailed in Table 3) before to be introduced in the system.

Chemical components	Mass percentage
Total Nitrogen (N)	19 %
Phosphorus Pentoxide (P_2O_5) soluble in neutral ammonium citrate and in water	19 % (8.3%P)
Phosphorus Pentoxide (P_2O_5) soluble in water	19 % (8.3%P)
Potassium Oxide	19 % (15.8% K)
Boron (B) soluble in water	0.15% 0.013%
Total Copper (Cu)	0.025%
Total Iron (Fe)	0.05%
Total Zinc (Zn)	0.009%
Total Manganese (Mn)	0.025%

Table 3: Chemical components of the soluble plant feed - Vitafeed 111 (Vitax company)

Observation tools and image processing

3D tomography volumes are acquired using the x-ray scanner at Laboratoire 3SR, specifically designed by RX-Solutions (Annecy, France). Each sample is scanned at 135 kV source voltage with a 0.2 mm copper filter; two vertically-stacked scans of 1120 projections (each 1536×1920) are acquired at a pixel size of 40 μm, the entire process takes just under 2 h. The acquires radiographs are reconstructed into a 3D volume using the software X-Act provided by the system manufacturer.

The first tomography is performed the day when the seedling in placed in the sand sample, thereafter each sample is scanned at 24 h intervals, in this work the evolution of the seed-sand

sample is scanned eight times. This time is sufficient to obtain a root system with embryonic roots such primary and seminals, as well as post-embryonis, laterals and crown roots (Hochholdinger 2009) (Figure 2) for both sand densities studied.

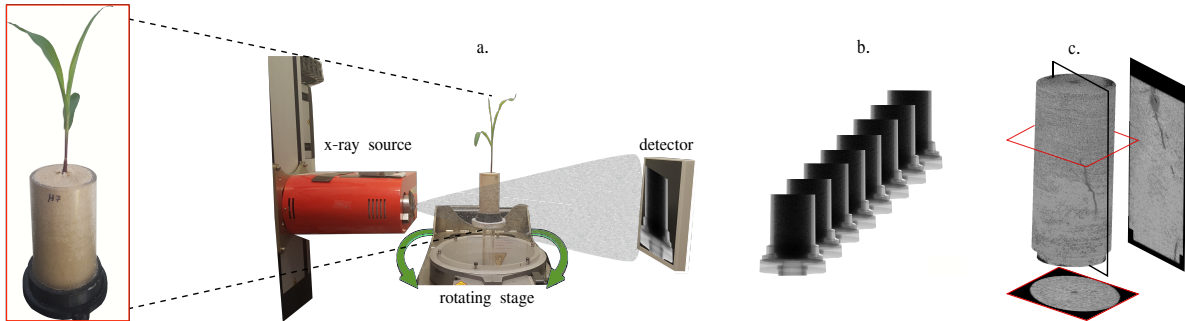Figure 1 summarises the steps followed to obtain the 3D reconstruction of the specimens.

Figure 1: Steps for sample tomography; a. x-ray setup, b. 2D radiographies, c. 3D reconstruction

A specifically designed image segmentation technique based on variance and bilateral filtering as well as thresholding is used to identify the root growth into the sand sample (Anselmucci et al. 2019). Figure 2 shows root systems extracted from the tomographies for denser and looser sand states. The mean root diameter ϕ_R, in both cases, is $0.57 \pm 0.1\,\text{mm}$, however the effect of the sand density on the development of the root system is clearly visible. The elements composing the root system are concentrated in the upper part of the denser sand sample whereas the whole height of looser sand sample is investigated by the root system.
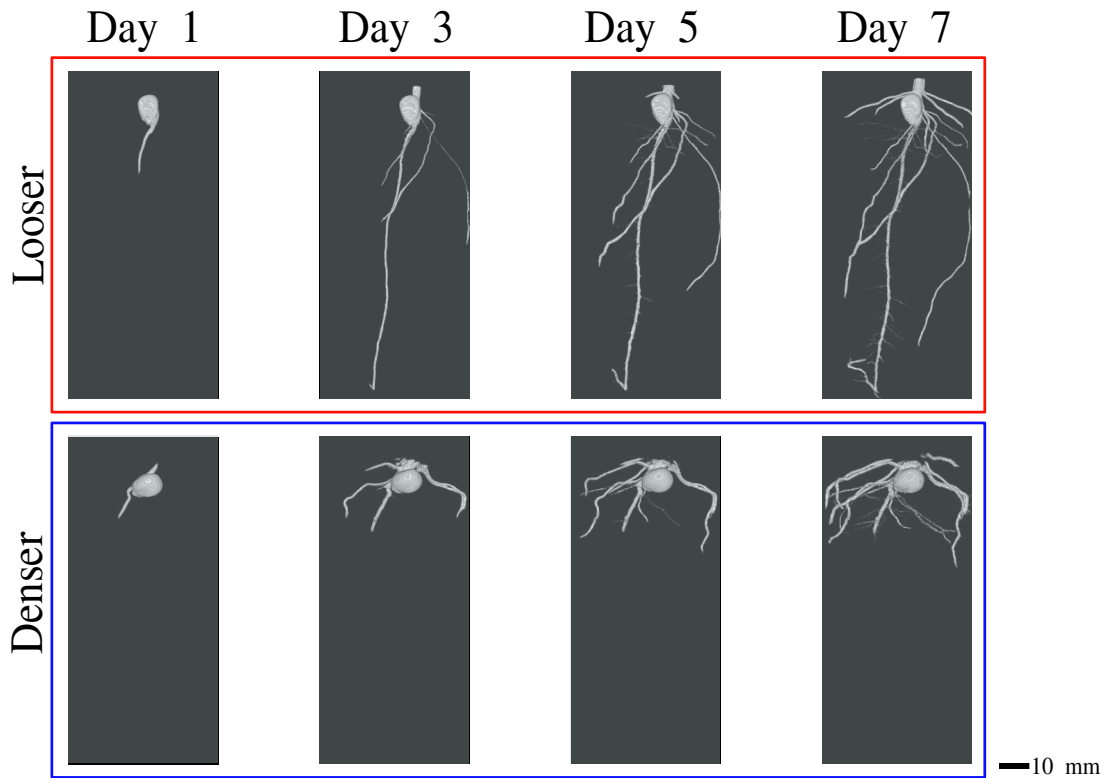

Figure 2: Maize root systems evolution on selected days for looser and denser sand specimens

Digital Volume Correlation (DVC) is used to measure rearrangements between two imaged states. Given two textured 3D volumes of with small rearrangements, DVC entails the optimised search for a transformation function that best matches the volumes. In this work a *local* approach is used, whereby the reference (initial) 3D image is split into regular cubes whose dimension is set such that there is sufficient texture to be able to match changes, and independent linear transformation functions are solved for for each cube.

The reconstructed images are binned $2 \times 2 \times 2$ the pixel size is consequently doubled to $80\,\mu m$ – this operation divides data volume by a factor 8 and also denoises significantly, at the (possible) cost of spatial resolution. The regular grid is composed of $40 \times 40 \times 99$ non-overlapping cubic correlation windows measuring $17 \times 17 \times 17$ voxels, *i.e.*, $1.36 \times 1.36 \times 1.36\,mm$. The local DVC code in the free and open-source software `spam` (Andò et al. 2017, Stamati et al. 2020) is used in this work.

Kinematics

Figure 3 presents 3D vectorial *displacement* fields where the displacement vector is extracted from the measured linear transformation function for each correlation window. Each displacement vector is the displacement from day 0 until the day shown, and each displacement vector is shown in the centre of its cube. Arrows are scaled by XXX and are also coloured according to a colour map which is also proportional to the length of the displacement vector. The identified root system is plotted in the same coordinate system in green.

For both densities, measured displacements are clearly situated around the roots, and the most significant displacements occur in the areas with higher root density.

It seems reasonable to conclude that displacements seem to be induced by the growing of the root system. The maximum displacement magnitude is about $0.95\,mm$ $[2.5, 3] \times D_{50}$ and $1.16\,mm$ $3.5 \times D_{50}$ for the looser and denser states, respectively. In the looser specimen, the main root keeps growing after reaching the bottom of the container (after day 4), producing displacements about twice the grain size.

Strains

Using the displacement field, the field of local strain invariants is computed in the finite strain framework using a 3D implementation of the method proposed by Geers et al. (1996) (using a spherical structuring element of radius two as implemented in `spam-regularStrain`). The first invariant – the volumetric strain – is denoted ε_v and is obtained from the determinant of the transformation gradient ($\mathbf{F}$) - 1. The second invariant – Euclidean norm of the deviatoric part of the strain tensor) representing the intensity of the shear deformation ε_q.

Horizontal projections of the total (*i.e.,* computed from day 0) deviatoric and volumetric strain fields are presented in Figure 4. The deviatoric strain plotted is a "maximum" projection, whereby the maximum value of deviatoric strain in the axis of observation is kept. In contrast, the volumetric plotted is the mean of the field in the axis of observation.

The deviatoric strain field shows that root produces shear strain around itself (Figure 4). Shear deformations are predominant around the root, they are initiated by the elongation of the root tip, but do not present significant evolution once the tip has passed. Below the root tip the deviatoric strain has a lower intensity than along the root. Similar behaviour is found by Keyes et al. (2016), studying the effect of maize root on soil.
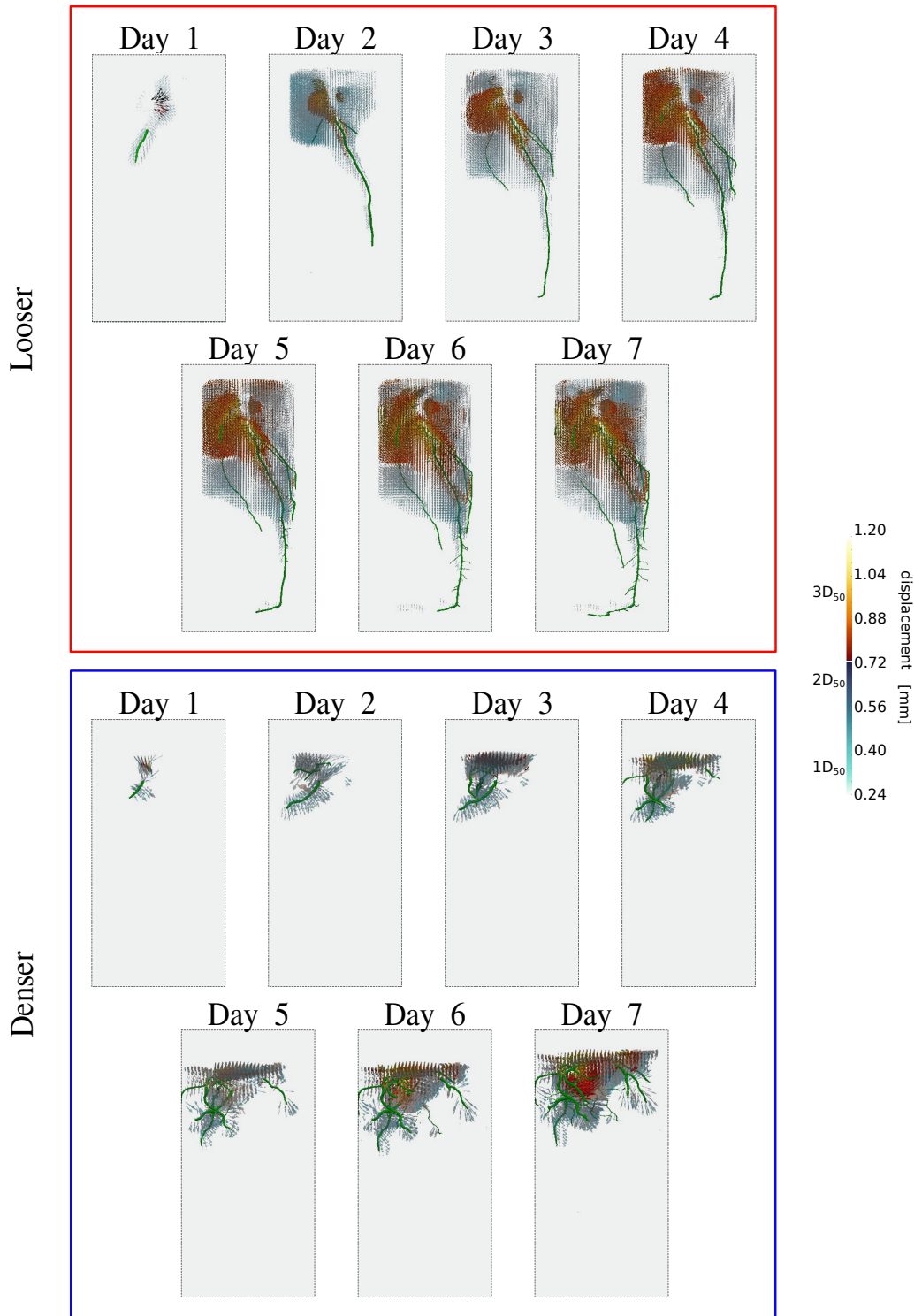
Figure 3: 3D rendering of vector plots (quiver plot) of the displacement fields, the colourmap and the arrow size indicate the magnitude of the total displacement measured in that correlation window. In green the root system is shown. For visualization purposes, displacements smaller than half D_{50} are not displayed. These rendering are made with ParaView (Ahrens et al. 2005)
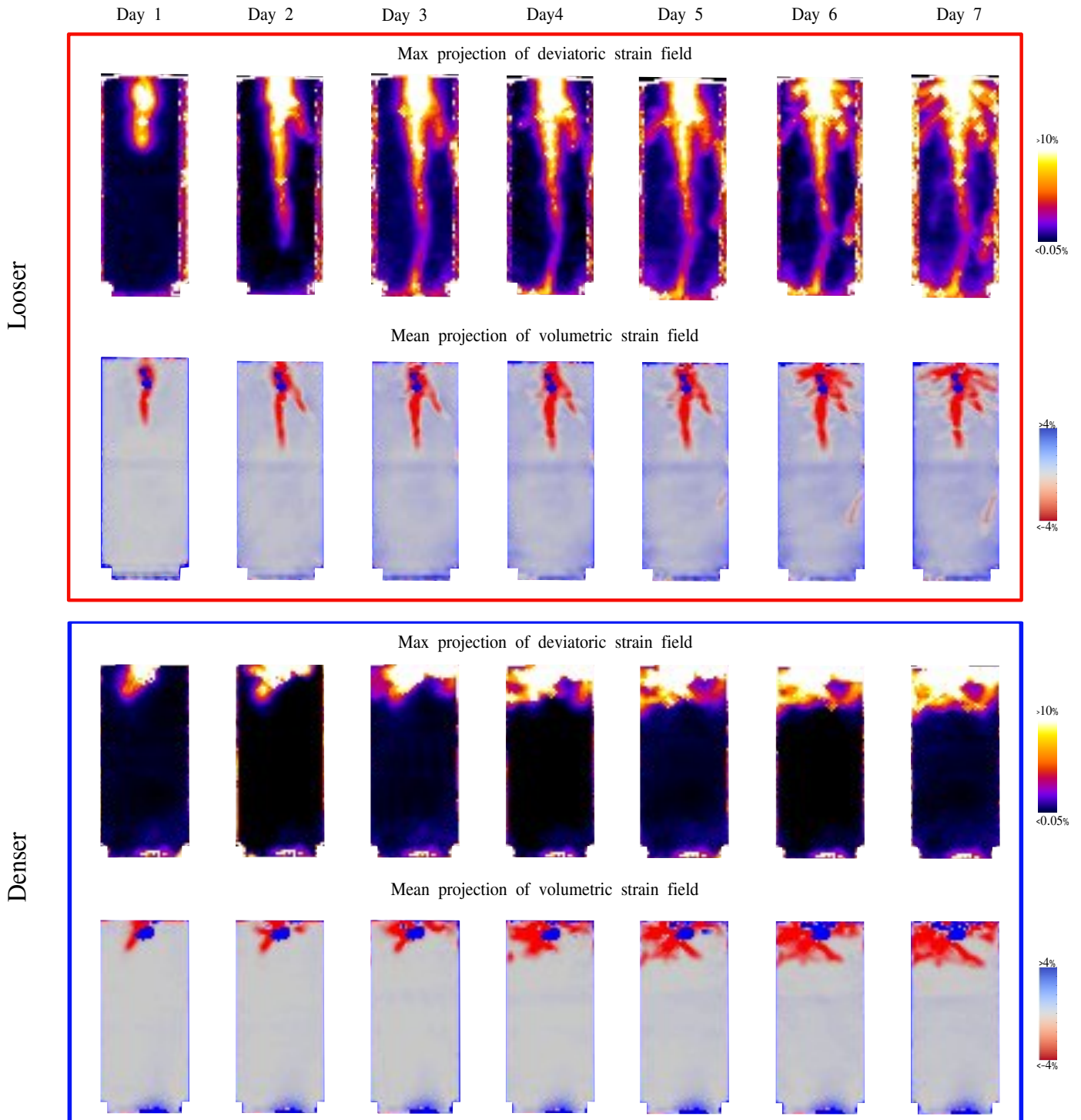
Figure 4: Projections of the total strain fields for looser and denser sand states. In each box, top row: maximum projection of the deviatoric strain reached at that time step, bottom row: average projection of the volumetric strain reached at that time step

Moving now to the volumetric strain field, dilation ($\varepsilon_{\mathrm{v}} < 0$) is also predominant at the vicinity of the roots which is partially in agreement with some previous analysis concerning the porosity changes in the rhizosphere (Bodner et al. 2014, Lucas et al. 2019). Further from the root system no

significant volume changes are identified for the denser specimen, whereas, in the looser specimen, the soil tends to compact. This behaviour is confirmed in a backup experiment on a similar loose sample.

The first 3 days of observation reveal that in the denser sample, dilation occurs radially up to 10-12 D_{50} from the root surface in the plane perpendicular to the root axis, while it propagates up to 14 D_{50} below the tip, but with a lower intensity. In the looser sample, the soil dilates up to a distance of 7.6-8 D_{50} from the root surface both radially and below the tip.

A volume of investigation around the root system is defined with respect to ε_q. Zones of higher shearing with $\varepsilon_q > 1\%$ are considered. Figure 5 gives examples of such shear zones of investigation marked out with the dotted green lines, superimposed with the volumetric strain field. The thickness of the sheared zone depends on the sand initial density, it is wider is the looser case ($\sim 10\,\phi_R$) than in the denser one ($\sim 8\,\phi_R$). Moreover, the volumetric strain field within the limit of the sheared zone presents different patterns. In the looser state both dilation and contraction are included, while no significant contraction is visible in the denser case. Volume changes in soils are mainly induced by shearing and are affected by the initial soil density. Therefore, ε_v is plotted in function of ε_q in Figure 6 for day 5. Each dot represents the couple $\varepsilon_v; \varepsilon_q$ computed in each correlation window. The displayed regression curve approximating the cloud of points show that sand dilation is clearly promoted by large ε_q for both densities (which occurs at the vicinity of the root - Figure 4). However, ε_v differs at low ε_q, with a slightly more contractant behaviour in the looser case (further from root). Indeed, the density function of the volumetric strain (Figure 6) shows that for lower intensity of ε_v, mostly contraction (positive ε_v) occurs in the looser specimen whereas dilation is slightly more predominant (negative ε_v) in the denser case.
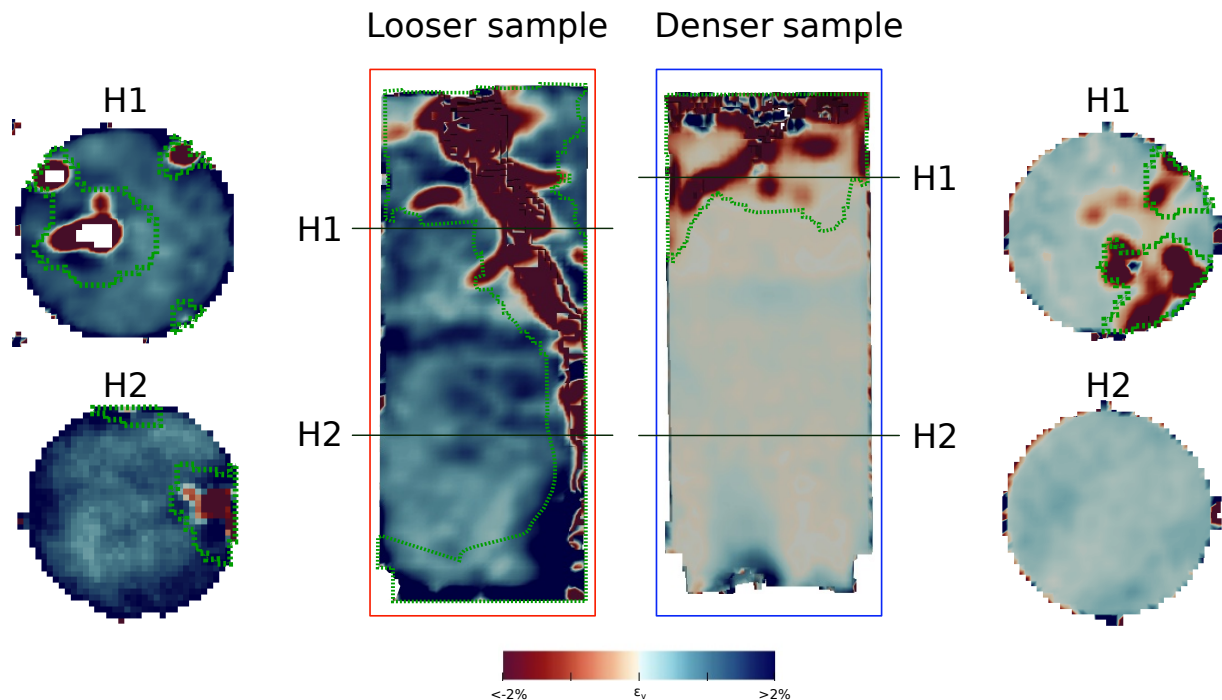

Figure 5: Vertical and horizontal sections of the volumetric strain field; Day 5. The dotted green line represents the contour of the sheared zone ($\varepsilon_q > 1\%$).
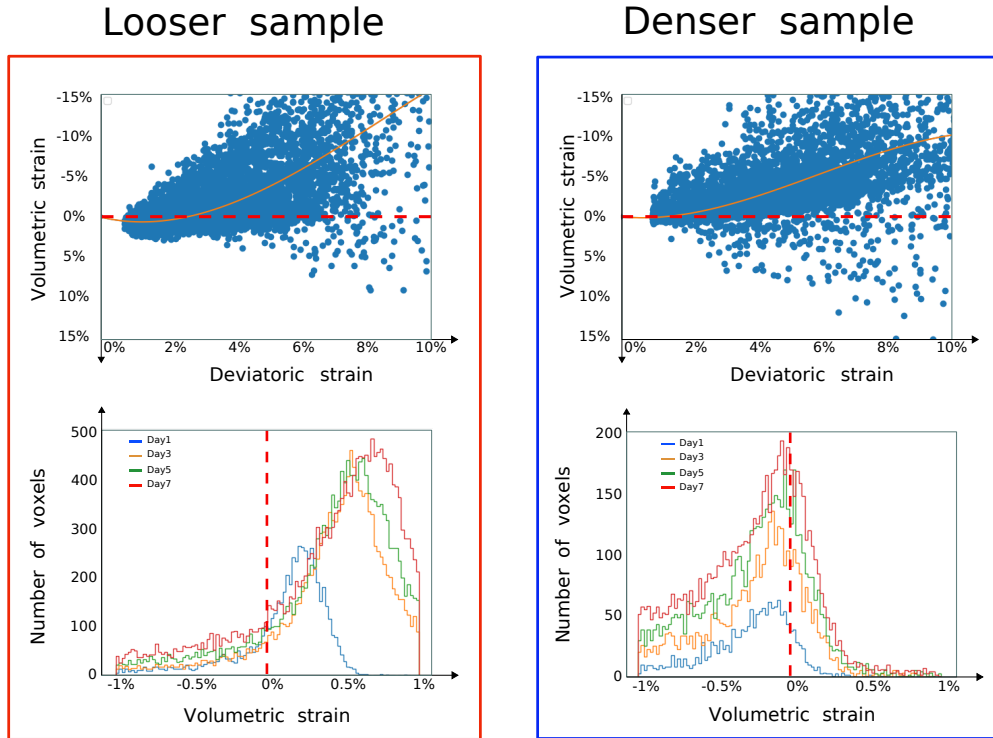
8

Figure 6: First row shows the ratio between deviatoric and volumetric strain, on Day 5 of the observation; Second row shows the density distribution evolution of the volumetric strain trend in the portion of soil engaged with a deviatoric strain >1%.

Conclusions

Soil deformations induced by root growth has been investigated in looser and denser sand samples. For the two density states high values of shear strain are found around the root system. The sheared sand volume ($\varepsilon_q > 1\%$) has a thickness of $\sim 10\phi_R$ in the looser configuration and $\sim 8\phi_R$ in the denser.

Nevertheless, soil response to root growth is strongly dependent on the initial density of the granular media. In the sheared volume, two different behaviours occur in terms of change of volume. In both states, close to the root the soil dilates. But, with the distance from the root, volumetric deformation tends to vanish in the denser case (at a radial distance of 10-12 D_{50}), whereas in the looser case soil compaction occurs at a distance 7.6-8 D_{50}. In addition, a relationship between deviatoric and volumetric strains is exhibited. The stronger the soil sheared by the root, the larger the soil volume change. Then, high soil porosity near the root may results not only from steric exclusion, as pointed in previous works, but also from the constitutive soil response to a shear deformation.

Further investigations with different bulk densities and grain size distributions are needed to find how plant root can affect soil response. Change of water content, and thus soil suction due to the root water uptake is also an important factor that should be considered. A clear understanding of the local mechanisms involved in root-soil interactions may constitute the base of a well founded constitutive relation for rooted soils with application for instance in slope stability or soil erosion.

Acknowledgements

References

Ahrens, J., Geveci, B. & Law, C. (2005), 'Paraview: An end-user tool for large data visualization', *The visualization handbook* **717**.

Andò, E., Cailletaud, R., Roubin, E. & Stamati, O. (2017), 'the spam contributors, spam: The software for the practical analysis of materials'.

Anselmucci, F., Andó, E., Sibille, L., Lenoir, N., Peyroux, R. & Arson, C. & Viggiani, G. . B. A. (2019), Root-reinforced sand: kinematic response of the soil, *in* '7th International Symposium on Deformation Characteristics of Geomaterials, IS-Glasgow 2019', EDP Sciences, p. 12011.

Bengough, A. G., McKenzie, B. M., Hallett, P. D. & Valentine, T. A. (2011), 'Root elongation, water stress, and mechanical impedance: a review of limiting stresses and beneficial root tip traits', *Journal of experimental botany* **62**(1), 59–68.

Bodner, G., Leitner, D. & Kaul, H. (2014), 'Coarse and fine rooted plant species have distinct effect on soil pore size distribution', *Plant and Soil* **380**.

Canou, J. (1989), 'Contribution à l'étude et à l'évaluation des propriétés de liquéfaction d'un sable', *Ph. D. Thesis, ENPC* .

Carminati, A. & Vetterlein, D. (2013), 'Plasticity of rhizosphere hydraulic properties as a key for efficient utilization of scarce resources', *Annals of botany* **112**(2), 277–290.

Flavigny, E., Desrues, J. & Palayer, B. (1990), 'Note technique: le sable d'hostun rf', *Revue française de géotechnique* (53), 67–70.

Geers, M., De Borst, R. & Brekelmans, W. (1996), 'Computing strain fields from discrete displacement fields in 2d-solids', *International Journal of Solids and Structures* **33**(29), 4293–4307.

Helliwell, J., Sturrock, C. J., Mairhofer, S., Craigon, J., Ashton, R., Miller, A., Whalley, W. & Mooney, S. J. (2017), 'The emergent rhizosphere: imaging the development of the porous architecture at the root-soil interface', *Scientific reports* **7**(1), 1–10.

Helliwell, J., Sturrock, C., Miller, A., Whalley, W. & Mooney, S. (2019), 'The role of plant species and soil condition in the structural development of the rhizosphere', *Plant, cell & environment* **42**(6), 1974–1986.

Hinsinger, P., Bengough, A., Vetterlein, D. & Young, I. (2009), 'Rhizosphere: biophysics, biogeochemistry and ecological relevance', *Plant and soil* **321**(1-2), 117–152.

Hochholdinger, F. (2009), The maize root system: morphology, anatomy, and genetics, *in* 'Handbook of maize: its biology', Springer, pp. 145–160.

Keyes, S., Cooper, L., Duncan, S., Koebernick, N., McKay Fletcher, D., Scotson, C., Van Veelen, A., Sinclair, I. & Roose, T. (2017), 'Measurement of micro-scale soil deformation around roots using four-dimensional synchrotron tomography and image correlation', *Journal of The Royal Society Interface* **14**(136), 20170560.

Keyes, S., Gillard, F., Soper, N., Mavrogordato, M., Sinclair, I. & Roose, T. (2016), 'Mapping soil deformation around plant roots using in vivo 4d x-ray computed tomography and digital volume correlation', *Journal of Biomechanics* **49**(9), 1802–1811.

Koebernick, N., Daly, K., Keyes, S., George, T., Brown, L., Raffan, A., Cooper, L., Naveed, M., Bengough, A., Sinclair, I. & Hallet, P. (2017), 'High-resolution synchrotron imaging shows that root hairs influence rhizosphere soil structure formation', *New Phytologist* **216**(1), 124–135.

Lucas, M., Schlüter, S., Vogel, H. & Vetterlein, D. (2019), 'Roots compact the surrounding soil depending on the structures they encounter', *Scientific reports* **9**(1), 1–13.

Lynch, J. (1995), 'Root architecture and plant productivity.', *Plant physiology* **109**(1), 7.

Mooney, S., Pridmore, T., Helliwell, J. & Bennett, M. (2012), 'Developing x-ray computed tomography to non-invasively image 3-d root systems architecture in soil', *Plant and soil* **352**(1-2), 1–22.

Moreno-Espíndola, I., Rivera-Becerril, F., de Jesús Ferrara-Guerrero, M. & De León-González, F. (2007), 'Role of root-hairs and hyphae in adhesion of sand particles', *Soil Biology and Biochemistry* **39**(10), 2520–2526.

Stamati, O., Andò, E., Roubin, E., Cailletaud, R., Wiebicke, M., Pinzon, G., Couture, C., Hurley, R. C., Caulk, R., Caillerie, D., Matsushima, T., Bésuelle, P., Bertoni, F., Arnaud, T., Laborin, A. O., Rorato, R., Sun, Y., Tengattini, A., Okubadejo, O., Colliat, J.-B., Saadatfar, M., Garcia, F. E., Papazoglou, C., Vego, I., Brisard, S., Dijkstra, J. & Birmpilis, G. (2020), "spam': Software for practical analysis of materials', *Journal of Open Source Software* **5**(51), 2286.
URL: *https://doi.org/10.21105/joss.02286*

Tracy, S., Black, C., Roberts, J., McNeill, A., Davidson, R., Tester, M., Samec, M., Korošak, D., Sturrock, C. & Mooney, S. (2012), 'Quantifying the effect of soil compaction on three varieties of wheat (triticum aestivum l.) using x-ray micro computed tomography (ct)', *Plant and Soil* **353**(1-2), 195–208.

White, R. & Kirkegaard, J. (2010), 'The distribution and abundance of wheat roots in a dense, structured subsoil–implications for water uptake', *Plant, cell & environment* **33**(2), 133–148.